Fourier Domain Gradient Descent Total Least Square/Fourth Algorithm for Efficient Adaptive Direction of Arrival Estimation

Joel S., *Graduate Student Member, IEEE*, Shekhar Kumar Yadav, *Member, IEEE*, Munukutla L. N. Srinivas Karthik, and Nithin V. George, *Member, IEEE*

***Abstract*—Direction-of-arrival (DOA) estimation is formulated within an adaptive-filtering framework that partitions the sensor array into a reference element and an auxiliary array. The auxiliary-array signal is filtered and subtracted from the reference to produce an error, minimized by the complex least-mean-square (LMS) algorithm. Although LMS converges rapidly with a large step size, it exhibits degraded steady-state performance; conversely, the complex least-mean-fourth (LMF) algorithm yields better steady-state accuracy but slower convergence. To combine their strengths, we propose two algorithms: complex LMS/F, which adaptively switches between LMS and LMF algorithms according to a threshold parameter; and complex GD-TLS/F, which employs a gradient-descent total-least-squares criterion to enhance robustness against noisy inputs. We derive the cost functions and weight update rules for both algorithms and introduce a novel computationally efficient Fourier domain approach for DOA estimation from the adaptive filter weights. A comprehensive theoretical analysis that includes a global optimal solution, mean stability, steady-state mean-square performance, and mean-square convergence is presented. Extensive simulation results demonstrate that the proposed algorithms achieve lower estimation error compared to existing adaptive algorithms.**

***Index Terms*—Adaptive DOA estimation, array signal processing, complex LMS, complex LMF, comple GD-TLS, complex GD-TLF, steady-state analysis.**

I. Introduction

DIRECTION-OF-ARRIVAL (DOA) estimation is the process of determining the angles or directions from which signals arrive at an array of sensors. By analyzing the signals received at different sensors and their time delays, amplitudes, or phase differences, it is possible to estimate the DOAs of the signal sources relative to the sensor array. This information can be crucial in various applications, such as tracking moving objects, locating targets, beamforming in wireless communication, and spatial filtering in audio processing. Traditionally, DOA estimation is performed using high-resolution algorithms like MUSIC [1], [2], [3] and ESPRIT [4], [5]. However, these algorithms are computationally expensive as they involve subspace-based processing that relies on eigenvalue decomposition. These subspace-based algorithms also need to know the total number of sources apriori to estimate the DOAs. DOA estimation methods based on the maximum likelihood estimation approach and sparse Bayesian learning approach have also been proposed [6], [7], [8], [9], [10], [11], [12], [13], but for these approaches, the probability distribution of the signals and the noise have to be known in advance. Sparse recovery, compressed sensing and dictionary learning based approaches have also been introduced for DOA estimation in the literature [14], [15], [16], [17], [18], [19], but these algorithms work by solving a convex semi-definite programming (SDP) problem, which is not suitable for low-powered implementation. Atomic norm minimization (ANM) based approaches have also been proposed for DOA estimation [20], [21], [22], [23], [24], but these techniques, in addition to being computationally complex, are also only applicable to uniform arrays and cannot be applied to arbitrarily shaped arrays.

To reduce the computational complexity of DOA estimation, a recent approach in [25] introduced an adaptive method using the LMS principle. This method used the instantaneous signals captured by the array to update an adaptive filter iteratively. The iterative process facilitated the weights of the adaptive filter to learn the delay information of the source signals among the elements of the array. The converged filter weight with sufficient learning was then used to estimate the DOAs. This adaptive approach provides a computationally efficient alternative to the subspace-based and other techniques by eliminating the need for eigenvalue decomposition of the array covariance matrix and not requiring solving any convex optimization problem. In addition, the adaptive approach doesn't require prior knowledge of the number of sources. Further, various extensions, such as a variable step-size (VSS) LMS algorithm for enhanced DOA estimation in noisy conditions [26], a VSS-LMS algorithm that improves performance when signals are affected by Gaussian noise using the total least squares (TLS) technique [27], and an

Received 18 December 2024; revised 18 May 2025 and 12 July 2025; accepted 10 August 2025. Date of publication 14 August 2025; date of current version 13 February 2026. This work was supported in part by the Department of Science and Technology, Government of India, through the MATRICS Scheme under Grant MTR/2022/000290, and in part by the TEOCO Chair of the Indian Institute of Technology Gandhinagar. The review of this article was coordinated by Prof. Jun Won Choi. *(Corresponding author: Joel S.)*

Joel S., Munukutla L. N. Srinivas Karthik, and Nithin V. George are with the Department of Electrical Engineering, Indian Institute of Technology Gandhinagar, Gandhinagar 382355, India (e-mail: joel.s@iitgn.ac.in; karthik_munukutla@iitgn.ac.in; nithin@iitgn.ac.in).

Shekhar Kumar Yadav was with the Department of Electrical Engineering, Indian Institute of Technology Gandhinagar, Gandhinagar 382355, India. He is now with Audio Information Processing Lab, Technical University of Munich (TUM), 80333 München, Germany (e-mail: yadav_shekhar@iitgn.ac.in).

Digital Object Identifier 10.1109/TVT.2025.3599310

adaptive algorithm based on the exponential hyperbolic cosine function for robust DOA estimation in the presence of outliers [28], have been proposed. Other adaptive DOA estimation methods have also been introduced to handle different sensing environments, array impairments, and underdetermined DOA estimation in recent literature [29], [30], [31], [32], [33], [34], [35], [36], [37], [38].

To improve the steady-state performance of mean square error adaptive algorithms, Walach and Widrow proposed the LMF algorithm in their work in [39]. In contrast to the squared power employed in the traditional LMS algorithm, the LMF algorithm utilized the fourth-order power of the error signal. This enabled the LMF algorithm to achieve low steady-state error. To take advantage of both the LMS and LMF algorithms, a combined LMS/F algorithm was proposed for the task of system identification in [40]. The LMS/F algorithm has also found applications in active noise control [41] and sparse channel estimation [42].

In this paper, we propose a family of two least square/fourth adaptive algorithms to estimate the DOAs of signals. The first proposed algorithm is a complex LMS/F algorithm. As far as we know, no previous research on DOA estimation has used any LMS/F based algorithm. We present the cost function of the complex LMS/F algorithm and derive an update rule for the weights of the proposed filter. Depending on a threshold parameter, the proposed update rule can switch between the complex LMS and complex LMF algorithms. This allows our algorithm to exploit the advantages of both the least square/fourth algorithms. To deal with scenarios where the input and output signal of the array is noisy, we propose a second algorithm called the complex gradient descent TLS/F (GD-TLS/F) algorithm. Once again, we present the cost function of GD-TLS/F and derive the weight update rule. The condition determining when the proposed algorithm switches between GD-TLS and GD-TLF is also presented. To the best of our knowledge, there is no existing research on the proposed GD-TLS/F adaptive algorithm for any applications.

After obtaining the final weights, we also introduce a novel and efficient way to estimate the DOAs from the weight vector that does not require the computationally expensive grid search. In one of our previous works [34], we introduced a polynomial rooting technique to estimate the DOAs from the filter weights in an efficient manner. To further reduce the computational efficiency of obtaining the DOAs from the adaptive filter weights, in this work, we utilize the fact that the steering vector of a uniform linear array is periodic with a period 2π to obtain the DOAs based on a Fourier domain analysis of the weight vector. This proposed method can be implemented using the efficient Fast Fourier Transform (FFT) method and does not require extensive grid search or solving a polynomial. Further, a detailed theoretical analysis of the proposed adaptive array signal processing algorithm is presented, which includes deriving the global optimal solution, mean stability, steady-state mean square performance and the mean square convergence analysis of the algorithm. Finally, the performance of the proposed algorithms is verified through extensive DOA estimation simulations. The main contributions of the paper are as follows:

1) Development of a novel complex GD-TLS/F algorithm for multichannel signal processing: We propose a complex gradient descent Total Least Squares/Fourth (GD-TLS/F) algorithm, designed for the multichannel signal case. This algorithm extends the conventional LMS/F framework and is particularly effective in scenarios where the signals are contaminated with additive Gaussian noise.
2) Derivation of multichannel adaptive weight update equations for complex LMS/F and complex GD-TLS/F algorithm: We derive the complete adaptive weight update equations for both complex LMS/F and the proposed complex GD-TLS/F algorithms in a multichannel scenario. These update rules allow the proposed filters to adaptively learn from the incoming signal snapshots and the error signal.
3) Comprehensive theoretical performance analysis of the proposed algorithm is thoroughly analyzed from a theoretical standpoint. Specifically, we:
   - Obtained the globally optimal solution for the filter weights.
   - Derived the mean stability conditions which helps us define the range of the step size (μ) of the adaptive filter for which the algorithm is convergent.
   - Obtained the steady-state mean square error.
   - Analysed the mean-square convergence behaviour of the algorithm.
4) Mathematical formulation and implementation of computationally efficient spatial spectrum estimation using Fourier Domain Processing: We propose a novel method for spatial spectrum estimation in the Fourier domain as an alternative to grid search-based approaches used in adaptive algorithms. The Fourier-based method reduces computational complexity significantly. We formulated the spatial spectrum estimation problem in the Fourier domain and derived the associated mathematical expressions for efficient computation. This includes the definition of the Fourier transform of the array manifold and its role in resolving the DOA spectrum without exhaustive angular scanning.

The structure of the paper is outlined as follows: Section II provides a review of the preliminaries of adaptive DOA estimation. Section III presents a detailed explanation of the proposed algorithms and a novel technique to estimate the spatial spectrum from the weights of the adaptive filter to estimate the DOAs. Section IV presents the derivation of the global optimal solution, mean stability, steady-state mean square performance, and mean square convergence analysis of the proposed algorithm. Section V presents simulations and discussions, while Section VI concludes the paper.

Notation: Matrices are denoted by bold uppercase characters, while vectors are represented by bold lowercase characters. The complex conjugate, transpose, and conjugate transpose are denoted by subscripts $(.)^*$, $(.)^{\mathrm{T}}$, and $(.)^{\mathrm{H}}$, respectively. $\mathbb{E}(.)$ is the expectation operator, tr$(\cdot)$ denotes the trace of a matrix, $||.||$ represents the ℓ_2-norm of a vector and $|\cdot|$ represents the absolute value of a complex number.

II. Preliminaries

Our work aims to estimate the DOAs of L narrowband and uncorrelated signals received by a uniform linear array (ULA) with M elements ($L < M$). The M elements of the array are placed at md, where $m = 0, 1, \ldots, M-1$, and d is the unit spacing between the elements. The ULA's first element (placed at the origin) serves as the reference element with respect to which the propagation delays of the other elements are calculated. The rest of the elements are referred to as auxiliary array elements. The signal received by the reference array element at the k^{th} time instance, denoted as $x_0(k)$, can be written as

$$x_0(k) = \sum_{l=1}^{L} s_l(k) + n_0(k) = y_0(k) + n_0(k). \tag{1}$$

Here, $n_0(k)$ represents the additive noise in the reference element, and $y_0(k) = \sum_{l=1}^{L} s_l(k)$ is the sum of all the L incoming signals $s_l(k)$ at the reference element without any delay. The signal captured by the auxiliary array can be expressed as

$$\boldsymbol{x}(k) = \sum_{l=1}^{L} s_l(k)\mathbf{v}(\theta_l) + \mathbf{n}(k) = \boldsymbol{y}(k) + \mathbf{n}(k), \tag{2}$$

where, the vector $\mathbf{v}(\theta_l) = [e^{-j\frac{2\pi}{\lambda}d\sin\theta_l}, e^{-j\frac{2\pi}{\lambda}2d\sin\theta_l}, \ldots, e^{-j\frac{2\pi}{\lambda}(M-1)d\sin\theta_l}]^{\mathrm{T}}$ represents the steering vector corresponding to the auxiliary array, containing the delay information of the l^{th} signal. λ is the wavelength of the narrowband signal and we keep $d = \frac{\lambda}{2}$ to avoid spatial aliasing. The set $\{\theta_1, \theta_2, \ldots, \theta_L\} \in [-90^\circ, 90^\circ]$ represents the DOAs of the L sources, and $\mathbf{n}(k)$ represents noise in the auxiliary array channels. To formulate the DOA estimation as an adaptive filtering problem, the signals captured by the auxiliary array elements are passed through an adaptive filter weight vector $\boldsymbol{w}(k) \in \mathbb{C}^{(M-1)\times 1}$ to produce the signal $f(k) = \boldsymbol{w}^{\mathrm{H}}(k)\boldsymbol{x}(k)$ at the output of the filter. The output signal of the filter is then compared to the signal received by the reference element, resulting in an error signal as

$$\zeta(k) = x_0(k) - \boldsymbol{w}^{\mathrm{H}}(k)\boldsymbol{x}(k). \tag{3}$$

This error signal is minimized so that the weight vector can learn the delay information between the reference element and the auxiliary array, which depends on the DOAs of the sources. Following adaptive filter theory, the weights are optimized by minimizing the Mean-Square Error (MSE) cost function

$$J\left[\boldsymbol{w}(k)\right] = \mathbb{E}[|\zeta(k)|^2/2]. \tag{4}$$

From (1) and (2), we observe that this cost function is minimized when the optimized weight satisfies the condition $\boldsymbol{w}^{\mathrm{H}}(k)\mathbf{v}(\theta_l) \approx 1$ for all $l \in \{1, 2, \ldots, L\}$. This condition is eventually used to estimate the DOAs from the optimized weight vector. We now discuss two existing algorithms that optimize the filter weights $\boldsymbol{w}$ in an adaptive manner:

Complex LMS: The complex LMS adaptive algorithm approximates the MSE in (4) using instantaneous squared values as $J[\boldsymbol{w}(k)] = |\zeta(k)|^2/2$, resulting in the following weight update rule

$$\boldsymbol{w}(k+1) = \boldsymbol{w}(k) - \mu\frac{\partial J}{\partial \boldsymbol{w}(k)} = \boldsymbol{w}(k) + \mu\zeta^*(k)\boldsymbol{x}(k), \tag{5}$$

where μ is referred to as the step size.

Complex LMF (Least Mean Fourth): The cost function of the complex LMF adaptive algorithm is based on the fourth moment of the error signal and is defined as

$$J\left[\boldsymbol{w}(k)\right] = \mathbb{E}[|\zeta(k)|^4/4]. \tag{6}$$

The weight update rule of complex LMF is given by

$$\boldsymbol{w}(k+1) = \boldsymbol{w}(k) + \mu\zeta^*(k)|\zeta(k)|^2\boldsymbol{x}(k). \tag{7}$$

Once the final weight $\boldsymbol{w}$ has been determined by the adaptive process, we create a modified weight vector $\boldsymbol{w}_a$, defined as $\boldsymbol{w}_a = [1, -\boldsymbol{w}^{\mathrm{T}}]^{\mathrm{T}} \in \mathbb{C}^{M\times 1}$. Subsequently, we calculate the spatial spectrum at every possible angular grid point θ using the following formula

$$\mathcal{S}(\theta) = \frac{1}{|\boldsymbol{w}_a^{\mathrm{H}}\mathbf{v}_a(\theta)|}, \tag{8}$$

where, $\mathbf{v}_a(\theta)$ is represented as $[1, \mathbf{v}^{\mathrm{T}}(\theta)]^{\mathrm{T}}$. The resulting $\mathcal{S}(\theta)$ exhibits a peak at the locations of the L DOAs as the condition $\boldsymbol{w}^{\mathrm{H}}\mathbf{v}(\theta_l) \approx 1$ (same as the condition $\boldsymbol{w}_a^{\mathrm{H}}\mathbf{v}_a(\theta_l) \approx 0$) is satisfied solely for the DOAs (θ_l) of the incoming signals.

In one of our previous works [34], instead of using the grid search method to calculate the spatial spectrum in (8), we introduced a computationally efficient gridless technique to find the DOAs. This method avoids searching the dense grid for DOA estimation and is called the off-grid polynomial rooting technique. Leveraging the structure of $\mathbf{v}_a$, we initially express $\mathbf{v}_a$ as $\mathbf{v}_a(\theta) = [1, z, z^2, \ldots, z^{(M-1)}]^{\mathrm{T}}$, where $z = e^{-j\pi\sin\theta}$. Subsequently, we represent the term in the denominator of $\mathcal{S}(\theta)$ as a polynomial in z as

$$Q(z) = \sum_{m=0}^{(M-1)} [\boldsymbol{w}_a]_{(m+1)} z^m, \tag{9}$$

where, $[\boldsymbol{w}_a]_m$ denotes the m^{th} element of the weight vector $\boldsymbol{w}_a$. It is evident that $Q(z)$ possesses $(M-1)$ roots around the unit circle. By determining the roots of $Q(z)$, we can estimate the DOAs using the relationship $\theta_l = \sin^{-1}(-\text{angle}(z_l)/2\pi)$, where, z_l corresponds to the L roots of $Q(z)$ that is closest to the unit circle.

III. Proposed Algorithm

In this section, we propose a family of two least square/fourth algorithms. First, we propose the complex LMS/F algorithm, and later, we propose a gradient descent based total Least square/fourth (GD-TLS/F) algorithm for adaptive DOA estimation. We also introduce a novel and efficient Fourier domain method for obtaining the DOAs from the weights of the adaptive filter.

A. Complex LMS/F Algorithm

The complex LMS/F algorithm takes advantage of the strengths of both complex LMS and complex LMF algorithms. This algorithm imitates complex LMS for faster initial convergence through a larger step size and complex LMF to attain reduced steady-state error by employing a smaller step size. The

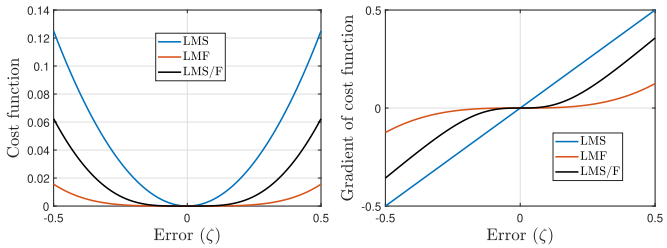

(a) (b)

Fig. 1. Variation of (a) the cost function and (b) the gradient of the cost function with respect to error ($\gamma = 0.1$).

complex LMS/F cost function [43] is expressed as

$$J = \mathbb{E}\left\{\frac{1}{2}|\zeta(k)|^2 - \frac{\gamma}{2}\ln\left(|\zeta(k)|^2 + \gamma\right)\right\}, \tag{10}$$

where, γ is a positive threshold that controls the convergence speed and steady-state performance. The variation of the cost function and the gradient of the cost function with respect to error are shown in Fig. 1(a) and (b), respectively. From the figures, we can see that when the error signal ζ is larger, the cost function imitates complex LMS, and when ζ is smaller and close to zero, the proposed cost function imitates complex LMF. This behaviour will become clear after we derive the weight update rule. The gradient of the instantaneous cost function can be expressed as

$$\begin{aligned}\frac{\partial J}{\partial \boldsymbol{w}(k)} &= \frac{\partial\left\{\frac{1}{2}|\zeta(k)|^2 - \frac{\gamma}{2}\ln\left(|\zeta(k)|^2+\gamma\right)\right\}}{\partial \boldsymbol{w}(k)} \\ &= -\zeta^*(k)\boldsymbol{x}(k) + \frac{\gamma}{(|\zeta(k)|^2+\gamma)}\zeta^*(k)\boldsymbol{x}(k) \\ &= -\frac{\zeta^*(k)|\zeta(k)|^2}{|\zeta(k)|^2+\gamma}\boldsymbol{x}(k). \end{aligned} \tag{11}$$

In the above derivation, we use the relation $\frac{\partial|\zeta(k)|^2}{\partial \boldsymbol{w}(k)} = -2\zeta^*(k)\boldsymbol{x}(k)$. Now, the weight update for the proposed complex LMS/F can be obtained as

$$\boldsymbol{w}(k+1) = \boldsymbol{w}(k) - \mu\frac{\partial J}{\partial \boldsymbol{w}(k)} = \boldsymbol{w}(k) + \mu\frac{\zeta^*(k)|\zeta(k)|^2}{|\zeta(k)|^2+\gamma}\boldsymbol{x}(k), \tag{12}$$

where, μ is the step size. When $|\zeta(k)|^2 \gg \gamma$, the $|\zeta(k)|^2$ term in the denominator of the gradient becomes dominant and the weight update in (12) follows complex LMS update rule. Whereas, when $|\zeta(k)|^2 \ll \gamma$, the γ term in the denominator of the gradient becomes dominant and the weight update in (12) follows complex LMF update rule with a step size of $\frac{\mu}{\gamma}$. Thus, the transition between the two algorithms depends on the error signal and γ. Faster convergence of the complex LMS algorithm and lower steady-state error of the complex LMF method can both be achieved in the proposed algorithm with the proper selection of the threshold parameter. After convergence of the update rule in (12), we get the final weight vector, which can be used to estimate the DOAs.

As there is noise in the input signal, to compensate for the noise bias, we next introduce the complex Gradient Descent Total Least Square/Fourth (GD-TLS/F) algorithm for efficient DOA estimation.

B. Complex GD-TLS/F Algorithm

To formulate the complex GD-TLS/F, we use the Rayleigh quotient of the weight vector, which is expressed as

$$r(\boldsymbol{w}_a, \boldsymbol{R_a}) = \frac{\boldsymbol{w}_a^{\mathrm{H}}(k)\boldsymbol{R_a}\boldsymbol{w}_a(k)}{\boldsymbol{w}_a^{\mathrm{H}}(k)\boldsymbol{w}_a(k)} = \frac{\mathbb{E}\left[|\zeta(k)|^2\right]}{\|\boldsymbol{w}_a(k)\|^2} \tag{13}$$

where $\boldsymbol{R}_a = \mathbb{E}[\boldsymbol{x_a}(k)\boldsymbol{x}_{\boldsymbol{a}}^{\mathrm{H}}(k)]$, $\boldsymbol{x_a}(k) = [x_0(k), \boldsymbol{x}^{\mathrm{T}}(k)]^{\mathrm{T}}$, $\boldsymbol{w}_a(k) = [1, -\boldsymbol{w}(k)^{\mathrm{T}}]^{\mathrm{T}}$. From (13), instead of using $\mathbb{E}[|\zeta(k)|^2]$, we use $\frac{\mathbb{E}[|\zeta(k)|^2]}{\|\boldsymbol{w}_a(k)\|^2}$ to obtain the following GD-TLS/F cost function.

$$J = \mathbb{E}\left\{\frac{1}{2}\frac{|\zeta(k)|^2}{\|\boldsymbol{w}(k)\|^2+\alpha} - \frac{\gamma}{2}\ln\left(\frac{|\zeta(k)|^2}{\|\boldsymbol{w}(k)\|^2+\alpha} + \gamma\right)\right\}, \tag{14}$$

where α is a constant to avoid division by zero. The corresponding weight update of complex GD-TLS/F can now be written as

$$\boldsymbol{w}(k+1) = \boldsymbol{w}(k) - \mu\frac{\partial J}{\partial \boldsymbol{w}(k)}, \tag{15}$$

where μ is the step size. This can be solved using the gradient descent approach as

$$\begin{aligned}\frac{\partial J}{\partial \boldsymbol{w}(k)} &= \frac{\partial\left\{\frac{1}{2}\frac{|\zeta(k)|^2}{\|\boldsymbol{w}(k)\|^2+\alpha} - \frac{\gamma}{2}\ln\left(\frac{|\zeta(k)|^2}{\|\boldsymbol{w}(k)\|^2+\alpha}+\gamma\right)\right\}}{\partial \boldsymbol{w}(k)} \\ &= \left\{\frac{|\zeta(k)|^2}{|\zeta(k)|^2+\gamma(\|\boldsymbol{w}(k)\|^2+\alpha)}\right\}\frac{\partial H}{\partial \boldsymbol{w}(k)}, \end{aligned} \tag{16}$$

where $\frac{\partial H}{\boldsymbol{w}(k)}$ is expressed as

$$\begin{aligned}\frac{\partial H}{\boldsymbol{w}(k)} &= \frac{\partial\left(\frac{1}{2}\frac{|\zeta(k)|^2}{\|\boldsymbol{w}(k)\|^2+\alpha}\right)}{\partial \boldsymbol{w}(k)} \\ &= \frac{-\boldsymbol{x}(k)\zeta^*(k)}{(\|\boldsymbol{w}(k)\|^2+\alpha)} - \frac{\boldsymbol{w}(k)|\zeta(k)|^2}{(\|\boldsymbol{w}(k)\|^2+\alpha)^2}. \end{aligned} \tag{17}$$

Substituting (17) in (16), the final gradient can be given by

$$\frac{\partial J}{\partial \boldsymbol{w}(k)} = \frac{-\boldsymbol{x}(k)\zeta^*(k)|\zeta(k)|^2(\|\boldsymbol{w}(k)\|^2+\alpha) - \boldsymbol{w}(k)|\zeta(k)|^4}{(\|\boldsymbol{w}(k)\|^2+\alpha)^2\{|\zeta(k)|^2+\gamma(\|\boldsymbol{w}(k)\|^2+\alpha)\}} \tag{18}$$

and the final weight update can be given by

$$\begin{aligned}\boldsymbol{w}(k+1) = \boldsymbol{w}(k) &+ \mu\frac{|\zeta(k)|^2(\boldsymbol{x}(k)\zeta^*(k)(\|\boldsymbol{w}(k)\|^2+\alpha)}{(\|\boldsymbol{w}(k)\|^2+\alpha)^3(\frac{|\zeta(k)|^2}{\|\boldsymbol{w}(k)\|^2+\alpha)}+\gamma)} \\ &+ \frac{\boldsymbol{w}(k)|\zeta(k)|^2)}{(\|\boldsymbol{w}(k)\|^2+\alpha)^3(\frac{|\zeta(k)|^2}{\|\boldsymbol{w}(k)\|^2+\alpha)}+\gamma)}. \end{aligned} \tag{19}$$

When $\frac{|\zeta(k)|^2}{\|\boldsymbol{w}(k)\|^2+\alpha} \gg \gamma$, the $\frac{|\zeta(k)|^2}{\|\boldsymbol{w}(k)\|^2+\alpha}$ term in the denominator of the gradient becomes dominant and the weight update in (12)

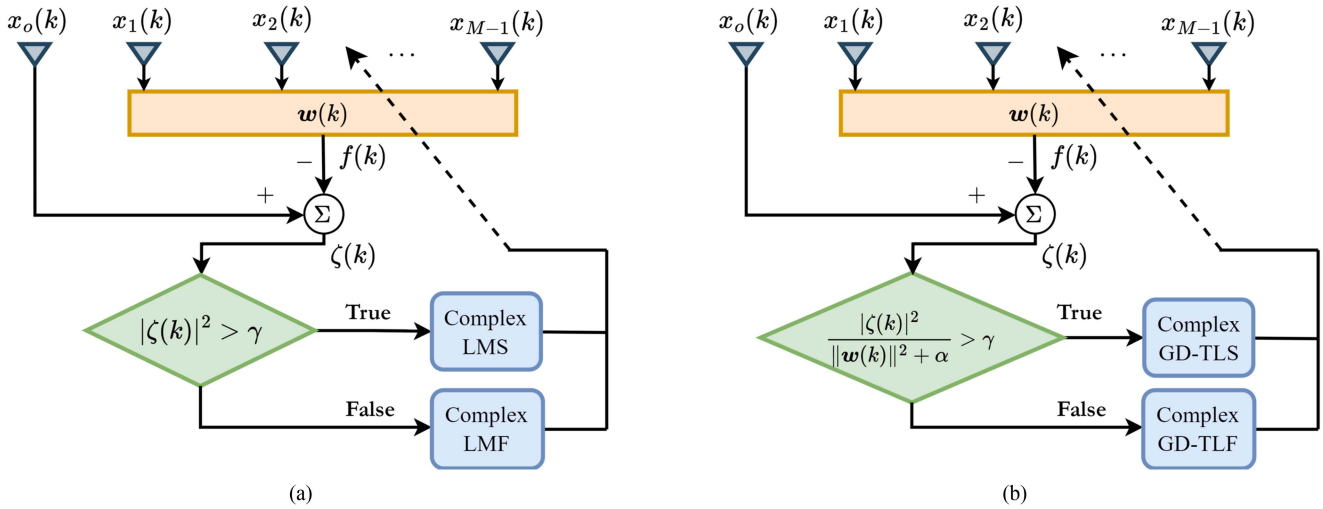

Fig. 2. Block diagram of the proposed (a) complex LMS/F and (b) complex GD-TLS/F adaptive DOA estimation algorithms.

follows complex GD-TLS update rule which can be expressed as

$$\boldsymbol{w}(k+1)=\boldsymbol{w}(k)+\mu\frac{\boldsymbol{x}(k)\zeta^*(k)(\|\boldsymbol{w}(k)\|^2+\alpha)+\boldsymbol{w}(k)|\zeta(k)|^2}{(\|\boldsymbol{w}(k)\|^2+\alpha)^2}. \tag{20}$$

Whereas, when $\frac{|\zeta(k)|^2}{\|\boldsymbol{w}(k)\|^2+\alpha} \ll \gamma$, the γ term in the denominator of the gradient becomes dominant and the weight update in (12) follows complex GD-TLF update rule with a step size of $\frac{\mu}{\gamma}$ which can be expressed as

$$\boldsymbol{w}(k+1) = \boldsymbol{w}(k) + \frac{\mu}{\gamma}\frac{|\zeta(k)|^2(\boldsymbol{x}(k)\zeta^*(k)(\|\boldsymbol{w}(k)\|^2+\alpha)}{(\|\boldsymbol{w}(k)\|^2+\alpha)^3} + \frac{\boldsymbol{w}(k)|\zeta(k)|^2)}{(\|\boldsymbol{w}(k)\|^2+\alpha)^3}. \tag{21}$$

The block diagrams of the proposed algorithms are shown in Fig. 2.

C. Fourier Domain Spectrum

In this section, we introduce a novel and computationally efficient Fourier domain method for obtaining the DOA spatial spectrum from the adaptive weight vector. From (8), the null spectrum of $\mathcal{S}(\theta)$, i.e. $b(\theta) = \boldsymbol{w}_a^{\mathrm{H}}\mathbf{v}_a(\theta)$, is periodic in θ with a period 2π. This is evident from the expression of the steering vector $\mathbf{v}_a(\theta)$. Thus, b can be expanded as a Fourier series as

$$b(\omega) = \sum_{m=-\infty}^{\infty} B_m e^{jm\omega}, \tag{22}$$

where B_m are the Fourier coefficients expressed as

$$B_m = \frac{1}{2\pi}\int_{-\pi}^{\pi} b(\omega)\, e^{-jm\omega} d\omega. \tag{23}$$

Comparing $b(\omega)$ with $b(\theta)$, we can see that $\omega = -\pi\sin\theta$ and $\{B_m\}_{m=0}^{M-1} = [\boldsymbol{w}_a]_{m=1}^{M}$. Hence, the Fourier series in (22) can be truncated to

$$b(\omega) = \sum_{m=0}^{M-1} [\boldsymbol{w}_a]_{m+1} e^{jm\omega}, \tag{24}$$

Thus, the null spectrum $b(\omega)$ can be obtained by the discrete Fourier transform (DFT) of the weight vector $\boldsymbol{w}_a$. The DFT can be calculated using the computationally efficient fast Fourier transform (FFT) method. To improve the resolution of the null spectrum, we pad zeros to the weight vector and write (24) as

$$b(n) = \sum_{m=0}^{N_{\mathrm{F}}} [\boldsymbol{w}_a]_{m+1} e^{j\frac{2\pi}{N_{\mathrm{F}}+1}nm}, \quad n = 0, 1, \ldots, N_{\mathrm{F}}, \tag{25}$$

where $N_{\mathrm{F}} \gg M-1$. After obtaining the $(N_{\mathrm{F}}+1)$-point FFT coefficients $b(n)$, we calculate the Fourier domain spectrum as

$$F(n) = \frac{1}{b(n)}, \quad n = 0, 1, \ldots, N_{\mathrm{F}}. \tag{26}$$

To obtain the DOAs, we map from the Fourier domain spectrum to the spatial spectrum. The mapping from the Fourier domain FFT points to the spatial spectrum domain is obtained as follows

$$\theta = \frac{180}{\pi} * \arcsin\left(\frac{n - 0.5 * N_{\mathrm{F}}}{0.5 * N_{\mathrm{F}}}\right), \tag{27}$$

where $n \in \{0, 1, \ldots, N_{\mathrm{F}}\}$ is the FFT point index ($N_{\mathrm{F}}+1$ is the total number of FFT points) and after mapping $\theta \in [-90°, 90°]$. After mapping, the peaks in the spatial spectrum correspond to the DOAs of the signals. When this method is used to estimate the DOAs using the weights of the proposed algorithms, we refer to the algorithms as Fourier domain complex LMS/F (FD complex LMS/F) and Fourier domain complex GD-TLS/F (FD complex GD-TLS/F), respectively.

The block diagram of Fourier domain spectrum estimation is shown in Fig. 3.

IV. Performance Analysis

In the following subsections, we derive the global optimal weight, mean stability, steady-state mean square performance,

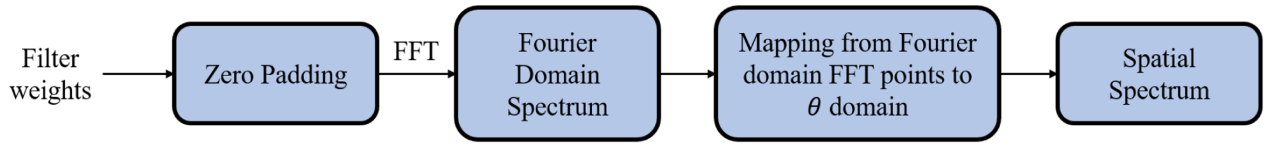

Fig. 3. Block diagram showing the steps to obtain the Fourier domain spectrum.

and the mean square convergence analysis using the methods in [44], [45], [46] of the proposed complex LMS/F adaptive algorithm. These derivations can be extended to the complex GD-TLS/F adaptive algorithm in a similar manner.

A. Global Optimal Solution

The cost function of the proposed complex LMS/F algorithm as introduced in (10) is once again

$$J = \mathbb{E}\left\{\frac{1}{2}|\zeta(k)|^2 - \frac{\gamma}{2}\ln\left[|\zeta(k)|^2+\gamma\right]\right\} \tag{28}$$

The optimal solution of the weight, when the algorithm reaches a steady state, can be derived by minimizing the cost function with respect to $\boldsymbol{w}(k)$, which is given as

$$\frac{\partial J}{\partial \boldsymbol{w}(k)} = \frac{\partial \mathbb{E}\left\{\frac{1}{2}|\zeta(k)|^2 - \frac{\gamma}{2}\ln\left[|\zeta(k)|^2+\gamma\right]\right\}}{\partial \boldsymbol{w}(k)} \tag{29}$$

$$= \frac{1}{2}\frac{\partial \mathbb{E}[|\zeta(k)|^2]}{\partial \boldsymbol{w}(k)} - \frac{\gamma}{2}\frac{\partial \mathbb{E}\{\ln\left[|\zeta(k)|^2+\gamma\right]\}}{\partial \boldsymbol{w}(k)}. \tag{30}$$

$$= \frac{1}{2}\frac{\partial \mathbb{E}[|\zeta(k)|^2]}{\partial \boldsymbol{w}(k)} - \frac{\gamma}{\mathbb{E}[|\zeta(k)|^2]+\gamma]}\frac{\partial \mathbb{E}[|\zeta(k)|^2+\gamma]\}}{\partial \boldsymbol{w}(k)} \tag{31}$$

The error corresponding to the optimal weight $\boldsymbol{w}_{\text{opt}}$ is $\zeta(k) = x_0(k) - \boldsymbol{w}_{\text{opt}}^{\text{H}}\boldsymbol{x}(k)$. As $\mathbb{E}[|\zeta(k)|^2] = \mathbb{E}[x_0(k)x_0^*(k)] - 2\boldsymbol{w}_{\text{opt}}^{\text{H}}\mathbb{E}[\boldsymbol{x}(k)x_0^*(k)] + \boldsymbol{w}_{\text{opt}}^{\text{H}}\mathbb{E}[\boldsymbol{x}(k)\boldsymbol{x}^{\text{H}}(k)]\boldsymbol{w}_{\text{opt}}$, (31) can be updated and set to zero as

$$\frac{\partial J}{\partial \boldsymbol{w}(k)} = -\boldsymbol{p} + \boldsymbol{R}_{\boldsymbol{x}}\boldsymbol{w}_{\text{opt}} - \frac{\gamma \boldsymbol{p}}{\mathbb{E}[|\zeta(k)|^2]+\gamma]} + \frac{\gamma \boldsymbol{R}_{\boldsymbol{x}}\boldsymbol{w}_{\text{opt}}}{\mathbb{E}[|\zeta(k)|^2]+\gamma]} = 0 \tag{32}$$

where $\boldsymbol{p} = \mathbb{E}[\boldsymbol{x}(k)x_0^*(k)]$ denotes cross correlation vector with $x_0^*(k)$ denoting the conjugate of the reference signal and $\boldsymbol{R}_{\boldsymbol{x}} = \mathbb{E}[\boldsymbol{x}(k)\boldsymbol{x}^{\text{H}}(k)]$ is the auto-covariance matrix of the auxiliary array signal $\boldsymbol{x}(k)$. On solving (32), the optimal solution can be obtained as

$$\boldsymbol{w}_{\text{opt}} = \boldsymbol{R}_{\boldsymbol{x}}^{-1}\boldsymbol{p}. \tag{33}$$

B. Mean Stability

The mean stability helps us define the range of the step size (μ) of the adaptive filter for which the algorithm is convergent. Using global optimal solution in (33) the weight error vector can be defined as $\boldsymbol{w}_e(k) = \boldsymbol{w}_{\text{opt}} - \boldsymbol{w}(k)$ and (12) is updated as

$$\boldsymbol{w}_e(k+1) = \boldsymbol{w}_e(k) - \mu\frac{\zeta^*(k)|\zeta(k)|^2}{|\zeta(k)|^2+\gamma}\boldsymbol{x}(k) \tag{34}$$

Taking expectation on both sides of (34) we get,

$$\mathbb{E}[\boldsymbol{w}_e(k+1)] = \mathbb{E}[\boldsymbol{w}_e(k)] - \mathbb{E}[\mu\beta(k)\zeta^*(k)\boldsymbol{x}(k)], \tag{35}$$

where $\beta(k) = \frac{|\zeta(k)|^2}{|\zeta(k)|^2+\gamma}$ and $\zeta(k) = \boldsymbol{w}_e^{\text{H}}(k)\boldsymbol{x}(k)$. Rearranging (35) we get,

$$\mathbb{E}[\boldsymbol{w}_e(k+1)] = \mathbb{E}[\boldsymbol{w}_e(k)]\mathbb{E}[(I - \mu\beta(k)\boldsymbol{R}_{\boldsymbol{x}}] \tag{36}$$

where $\boldsymbol{R}_{\boldsymbol{x}} = \mathbb{E}[\boldsymbol{x}(k)\boldsymbol{x}^{\text{H}}(k)]$ is once again the auxiliary array signal auto-covariance matrix. As the algorithm reaches steady state $\mathbb{E}[\boldsymbol{w}_e(k+1)] = \mathbb{E}[\boldsymbol{w}_e(k)]$. So, from (36), we can conclude that at convergence

$$\left|I - \mu\beta(k)\boldsymbol{R}_{\boldsymbol{x}}\right| \leq 1. \tag{37}$$

If $\rho_1, \rho_2, \ldots, \rho_N$ are the eigenvalues of $\boldsymbol{R}_{\boldsymbol{x}}$, then the range of μ from (37) should be

$$0 < \mu \leq \frac{1}{\beta(k)}\min\left(\frac{1}{\rho_1}, \frac{1}{\rho_2}, \ldots, \frac{1}{\rho_N}\right), \tag{38}$$

As we know that the maximum eigenvalue $\rho_{max} \leq \rho_1 + \rho_2 + \ldots + \rho_N$, so (38) can be written as

$$0 < \mu \leq \frac{1}{\beta(k)(\rho_1 + \rho_2 + \ldots + \rho_N)}. \tag{39}$$

The above expression can be simplified to find the range of step size for mean stability of the proposed algorithm as

$$0 < \mu \leq \frac{1}{\beta(k)\text{tr}(\boldsymbol{R}_{\boldsymbol{x}})}, \tag{40}$$

where $\text{tr}(\boldsymbol{R}_{\boldsymbol{x}}) = \rho_1 + \rho_2 + \ldots + \rho_N$.

C. Steady-State Mean Square Performance

In this subsection, we derive the steady-state mean square error (MSE) for the complex LMS/F algorithm. The noise-free error signal from (4) can be defined as

$$\zeta_{nf}(k) = y_0(k) - \boldsymbol{w}^{\text{H}}(k)\boldsymbol{y}(k) = \boldsymbol{w}_e^{\text{H}}(k)\boldsymbol{y}(k), \tag{41}$$

as $\boldsymbol{w}_{\text{opt}}^{\text{H}}\boldsymbol{y}(k) = x_0(k)$. Now, the relation between error signal $\zeta(k)$ and the error-free signal can be given by

$$\zeta(k) = \zeta_{nf}(k) + n_0(k) - \boldsymbol{w}^{\text{H}}\boldsymbol{n}(k), \tag{42}$$

where $\boldsymbol{n}(k)$ is the noise in the auxiliary array. The corresponding variance of (42) is written as

$$\sigma_\zeta^2 = \mathbb{E}[\zeta_{nf}^2(k)] + \sigma_0^2 + \sigma_n^2\mathbb{E}[||\boldsymbol{w}(k)||^2]. \tag{43}$$

where, σ_0^2 is the noise variance at reference sensor and σ_n^2 is the noise variance in the auxiliary array. To obtain $\mathbb{E}[\zeta_{nf}^2(k)]$, we once again write (34) as

$$\boldsymbol{w}_e(k+1) = \boldsymbol{w}_e(k) - \mu g[\zeta(k)]\boldsymbol{x}(k) \tag{44}$$

where $g[\zeta(k)] = \dfrac{\zeta^*(k)|\zeta(k)|^2}{|\zeta(k)|^2+\gamma}$. To further proceed with the analysis, the following assumptions have been made

1) An identical and independent distribution is followed by the noise $\mathbf{n}(k)$ which is independent of input $\boldsymbol{x}(k)$.
2) The noise free error signal $\zeta_{nf}(k)$ is independent of the noise $\mathbf{n}(k)$ and $||\boldsymbol{x}||^2$ is asymptotically uncorrelated to $g^2[\zeta(k)]$.

Applying the energy conservation relation to (44), we get the following relation

$$\begin{aligned}\mathbb{E}\left[||\boldsymbol{w}_e(k+1)||^2\right] &= \mathbb{E}\left[||\boldsymbol{w}_e(k)||^2\right] - 2\mu\mathbb{E}\left[\zeta(k)g[\zeta(k)]\right] \\ &\quad + \mu^2\mathbb{E}\left[g^2[\zeta(k)]||\boldsymbol{x}(k)||^2\right]\end{aligned} \tag{45}$$

Following the assumption (i) and (ii), (45) can be updated as

$$\begin{aligned}&\mathbb{E}\left[||\boldsymbol{w}_e(k+1)||^2\right] \\ &= \mathbb{E}\left[||\boldsymbol{w}_e(k)||^2\right] - 2\mu h_G[\zeta(k)]\mathbb{E}[|\boldsymbol{w}_e^{\mathrm{H}}(k)\boldsymbol{y}(k)|^2] \\ &\quad - 2\mu I_{M-1}\sigma_n^2\mathbb{E}[||\boldsymbol{w}_e||^2] + \mu^2\mathbb{E}\left[||\boldsymbol{x}(k)||^2\right]h_U[\zeta(k)]\end{aligned} \tag{46}$$

where, $h_G[\zeta(k)] = \dfrac{\mathbb{E}\{\zeta^*(k)g[\zeta^(k)]\}}{\mathbb{E}[\zeta^*(k)\zeta(k)]}$ and $h_U[\zeta(k)] = \mathbb{E}\{g^2[\zeta(k)]\}$. As the system reaches a steady state,

$$\lim_{k\to\infty}\mathbb{E}\left[||\boldsymbol{w}_e(k+1)||^2\right] \approx \lim_{k\to\infty}\mathbb{E}\left[||\boldsymbol{w}_e(k)||^2\right]. \tag{47}$$

As a result, (46) can be updated as follows

$$\lim_{k\to\infty}h_G[\zeta(k)]\lim_{k\to\infty}\mathbb{E}[|\boldsymbol{w}_e^{\mathrm{H}}(k)\boldsymbol{y}(k)|^2] = \tag{48}$$

$$\frac{\mu}{2}\mathbb{E}\left[||\boldsymbol{x}(k)||^2\right]\lim_{k\to\infty}h_U[\zeta(k)], \tag{49}$$

Now, noise-free steady-state MSE (η) is defined as

$$\lim_{k\to\infty}\mathbb{E}[\zeta_{nf}^2] = \lim_{k\to\infty}\mathbb{E}[|\boldsymbol{w}_e^{\mathrm{H}}(k)\boldsymbol{y}(k)|^2] \tag{50}$$

Based on (49), η can be updated as

$$\eta = \lim_{k\to\infty}\mathbb{E}[\zeta_{nf}^2] = \frac{\mu}{2}\mathrm{tr}(\boldsymbol{R}_{\boldsymbol{x}})\frac{\lim_{k\to\infty}h_U[\zeta(k)]}{\lim_{k\to\infty}h_G[\zeta(k)]}, \tag{51}$$

where

$$\lim_{k\to\infty}h_U[\zeta(k)] = \mathbb{E}\{g^2[\zeta(k)]\} = \beta^2(k)\mathbb{E}[\zeta(k)\zeta^*(k)] \tag{52}$$

and

$$\lim_{k\to\infty}h_G[\zeta(k)] = \beta(k). \tag{53}$$

Putting (52) and (53) in (51) we get,

$$\eta = \mu\gamma\mathrm{tr}(\boldsymbol{R}_{\boldsymbol{x}})(\eta + \sigma_0^2 + \sigma_n^2\mathbb{E}[||\boldsymbol{w}(\infty)||^2]). \tag{54}$$

Rearranging further, we get

$$\eta = \frac{\mu\gamma\mathrm{tr}(\boldsymbol{R}_{\boldsymbol{x}})(\sigma_0^2 + \sigma_n^2\mathbb{E}[||\boldsymbol{w}(\infty)||^2])}{2-\mu\gamma\mathrm{tr}(\boldsymbol{R}_{\boldsymbol{x}})}, \tag{55}$$

Based on (55) the steady-state MSE (κ) can be obtained as

$$\kappa = \sigma_0^2 + \frac{\mu\gamma\mathrm{tr}(\boldsymbol{R}_{\boldsymbol{x}})(\sigma_0^2+\sigma_n^2\mathbb{E}[||\boldsymbol{w}(\infty)||^2])}{2-\mu\gamma\mathrm{tr}(\boldsymbol{R}_{\boldsymbol{x}})} + \sigma_n^2\mathbb{E}[||\boldsymbol{w}(\infty)||^2] \tag{56}$$

D. Mean Square Convergence Analysis

Here, we analyze the mean square convergence behaviour of the proposed complex LMS/F algorithm. Based on (49), the condition that is sufficient to attain mean square stability can be expressed as

$$\mu \le \frac{2}{\mathbb{E}[||\boldsymbol{x}(k)||^2]}\inf_{\mathbb{E}[\zeta^2(k)]\in\Omega}\left[\mathbb{E}[||\boldsymbol{x}(k)||^2]\frac{h_G[\zeta(k)]}{h_U(\zeta(k))}\right], \tag{57}$$

Here, $\inf[.]$ represents the infimum, and the field Ω is expressed as [47],

$$\Omega = \left[\mathbb{E}[\zeta(k)^2] : \xi \le \mathbb{E}[\zeta(k)^2]\right] \tag{58}$$

where the parameter ξ represents a Cramer-Rao bound linked to estimating the random value $\boldsymbol{x}^{\mathrm{H}}(n)\boldsymbol{w}_{\mathrm{opt}}$ through the use of $\boldsymbol{x}^{\mathrm{H}}(n)\boldsymbol{w}(n)$. Considering assumptions (i) and (ii), along with the energy conservation relation in (45), we obtain

$$\begin{aligned}\mathbb{E}[||\boldsymbol{w}_e(k+1)||^2] &= \mathbb{E}[||\boldsymbol{w}_e(k)||^2] - \mu h_G[\zeta(k)]\mathrm{E}[|\boldsymbol{w}_e^{\mathrm{H}}(k)\boldsymbol{x}(k)|^2] \\ &\quad + \frac{\mu^2}{2}\mathbb{E}[||\boldsymbol{x}(k)||^2]h_U[\zeta(k)].\end{aligned} \tag{59}$$

Now, for guaranteed stability, the condition

$$\mathbb{E}[||\boldsymbol{w}_e(k+1)||^2] \le \mathbb{E}[||\boldsymbol{w}_e(k)||^2] \tag{60}$$

should be satisfied. Thus, (59) can be written as

$$-2\mu h_G[\zeta(k)]\mathbb{E}[|\boldsymbol{w}_e^{\mathrm{H}}(k)\boldsymbol{y}(k)|^2] + \mu^2\mathbb{E}[||\boldsymbol{x}(k)||^2]h_U[\zeta(k)] \le 0. \tag{61}$$

Considering (59) and (61), the range of the step size μ is given by

$$\mu \le \frac{2\mathbb{E}[\zeta^2(k)]h_G[\zeta(k)]}{\mathbb{E}[||\boldsymbol{x}(k)||^2]h_U[\zeta(k)]}. \tag{62}$$

From (62), the proposed algorithm should satisfy the following sufficient condition to guarantee convergence

$$\begin{aligned}\mu &\le \frac{2}{\mathbb{E}[||\boldsymbol{x}(k)||^2]}\inf_{\mathrm{E}[\zeta^2(k)]\ge\xi}\left[\mathbb{E}[\zeta^2(k)]\frac{h_G[\zeta(k)]}{h_U[\zeta(k)]}\right] \\ &= \frac{2\xi}{\mathrm{E}[||\boldsymbol{x}(k)||^2]\gamma(\xi+\sigma_0^2+\sigma_n^2\mathbb{E}[||\boldsymbol{w}(\infty)||^2])}.\end{aligned} \tag{63}$$

V. Computational Complexity

Table I shows that all proposed algorithms operate with linear computational complexity, $\mathcal{O}(M)$, so their cost grows only proportionally to the number of array elements. The proposed adaptive DOA estimation algorithms, complex LMS/F and complex GD-TLS/F, add only a slight computational overhead compared to the baseline complex LMS algorithm. However, although the proposed algorithm requires slightly more computation than the complex LMS, this additional cost delivers enhanced performance. The histograms in Fig. 4 show the computational

TABLE I
COMPUTATIONAL COMPLEXITY COMPARISON OF ADAPTIVE ALGORITHMS

	Operations		$\mathcal{K}=1$ (per iteration) , $M=12$	
Algorithm	Multiplications	Additions	Multiplications	Additions
complex LMS	$\mathcal{K}(2M-1)$	$\mathcal{K}(2M-2)$	23	22
complex GD-TLS	$\mathcal{K}(4M+1)$	$\mathcal{K}(4M-4)$	49	44
complex LMS/F	$\mathcal{K}(2M+1)$	$\mathcal{K}(2M-1)$	25	23
complex GD-TLS/F	$\mathcal{K}(4M+4)$	$\mathcal{K}(4M-3)$	52	45

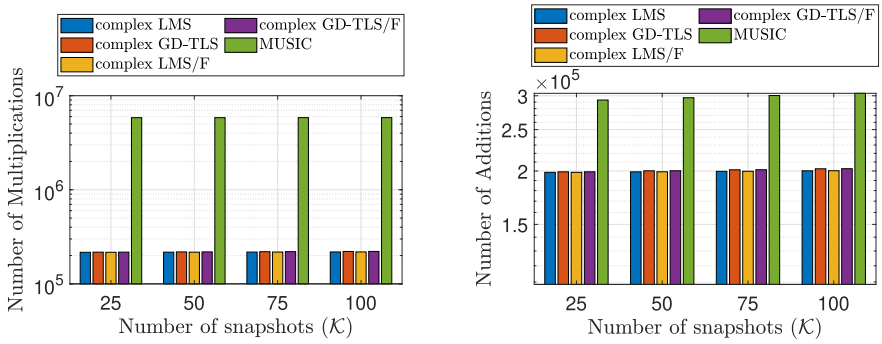

Fig. 4. Computational complexity in terms of the number of (a) Multiplications (b) Additions for $M=12$ of different algorithms.

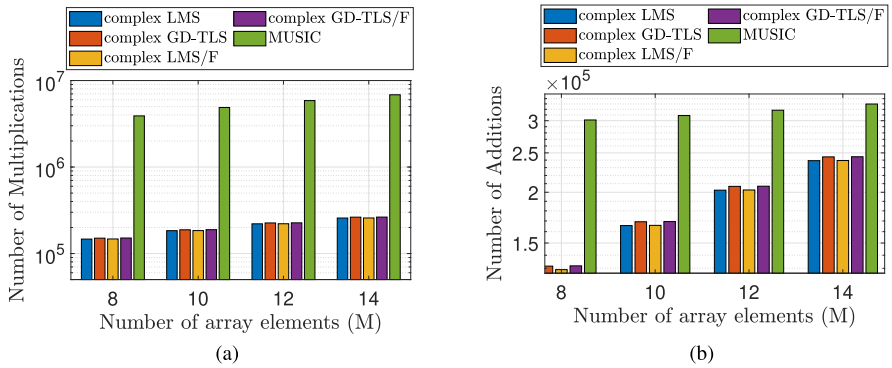

Fig. 5. Computational complexity in terms of the number of (a) Multiplications (b) Additions for $\mathcal{K}=200$ of different algorithms.

complexity with respect to snapshot count for $M=12$ and Fig. 5 shows the computational complexity with respect to array elements for $\mathcal{K}=200$. From both the figures, it can be seen that the computation of the subspace-based MUSIC algorithm dominates the computational cost. For the representative setting $M=12$ and $\mathcal{K}=200$, MUSIC demands 5,862,852 multiplications and 318,400 additions. By contrast, complex GD-TLS/F accomplishes the same task with only 226,412 multiplications and 207,011 additions. Complex GD-TLS/F reduces the number of multiplications by approximately 96.1% compared to the MUSIC algorithm and also requires approximately 35% fewer additions than the MUSIC algorithm. So, subspace-based techniques impose a much heavier computational load than the proposed adaptive algorithm, which limits their suitability for power-constrained environments. The core of this burden lies in the extensive matrix operations they require, such as eigenvalue decompositions and the formation of second-order statistics such as the covariance matrix. As a result, there is a direct trade–off between computational effort and estimation accuracy when opting for subspace methods. By contrast, the proposed adaptive framework works directly with first-order statistics and does not require EVD and covariance matrix calculations, reducing the computational requirements on both multiplications and additions. For $M=12$ and $\mathcal{K}=200$, the MUSIC algorithm alone demands an extra 5,636,440 multiplications compared to our proposed complex GD-TLS/F algorithm.

VI. SIMULATION AND DISCUSSION

In this simulation study, we examine the performance of various techniques in estimating the directions of different sources for two cases. In Case I, there are 4 sources with DOAs

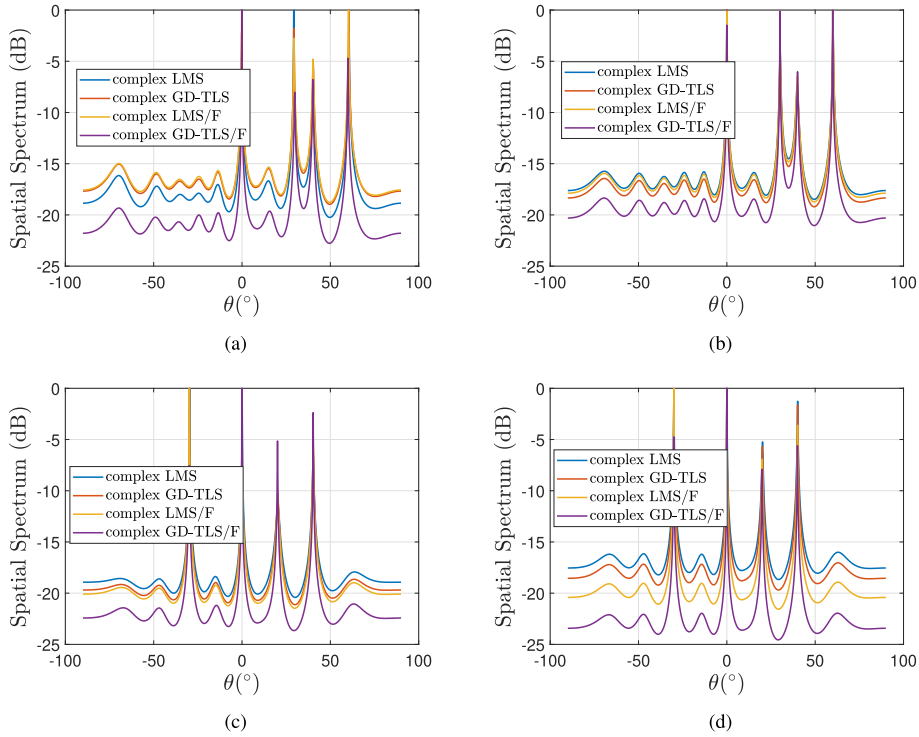

Fig. 6. (Case I) Spatial spectrum of complex LMS, complex GD-TLS, complex LMS/F and complex GD-TLS/F for (a) SNR = 6 dB and (b) SNR = 14 dB ($M = 12, \mathcal{K} = 500$). (Case II) Spatial spectrum of complex LMS, complex GD-TLS, complex LMS/F and complex GD-TLS/F for (c) SNR = 6 dB and (d) SNR = 14 dB ($M = 12, \mathcal{K} = 500$).

$\theta = 0°, 30°, 40°, 60°$ and in Case II, there are 4 sources with DOAs $\theta = -30°, 0°, 20°, 40°$. To perform these estimations, a ULA consisting of $M = 12$ elements is utilized. The step size for the complex LMS is $\mu = 0.008$, and for complex GD-TLS, it is $\mu = 0.6$. For complex LMS/F and complex GD-TLS/F, the step sizes are set to $\mu = 0.0075$ and $\mu = 0.032$, respectively. γ is set to 0.005 for both complex LMS/F and complex GD-TLS/F. The evaluation of these methods involves various simulations, which include the spatial and Fourier domain DOA spectrum plots, the mean squared error (MSE) convergence performance, and the root mean squared error (RMSE) performance of the estimated DOAs. To ensure the reliability of the results, all MSE plots are averaged over 10,000 Monte Carlo (MC) trials to achieve smoother curves, and RMSE plots are averaged over 2,000 MC trials.

A. *Analysis of Spatial Spectrum*

In Fig. 6, the spatial spectrum $\mathcal{S}(\theta)$ of all the algorithms are presented for Cases I and II for signal-to-noise ratios (SNRs) of 6 dB and 14 dB, respectively, with the number of snapshots set at $\mathcal{K} = 500$ for all the algorithms. The figure shows that the spatial spectrum of all the algorithms shows peaks at the locations of the DOAs of the sources.

The roots of the proposed complex GD-TLS/F method for cases I and II are shown in Fig. 7. The number of snapshots was set at 500, and all the figures were plotted for 200 Monte Carlo (MC) trials. The red stars in the figures indicate the roots closest to the unit circle, and we can see that the roots appear

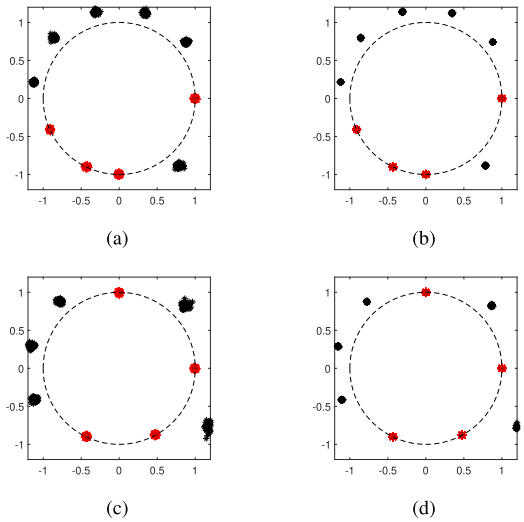

Fig. 7. (Case I) Roots of complex GD-TLS/F for (a) SNR = 6 dB and (b) SNR = 14 dB ($M = 12, \mathcal{K} = 500$). (Case II) Roots of complex LMS/F for (c) SNR = 6 dB and (d) SNR =14 dB ($M = 12, \mathcal{K} = 500$).

at the location of the DOAs of the sources for all the cases and SNRs. The estimated roots of complex GD-TLS/F with increasing snapshots are shown in Fig. 8 for 200 MC trials to show the adaptive process. Fig. 8(a) and (b) show the root plots for $\mathcal{K} = 10$ and 100 snapshots, respectively. The figure shows that as the number of snapshots increases, the estimated roots come closer to the desired DOA root location (shown in black circles), highlighting the convergence of the adaptive algorithm.

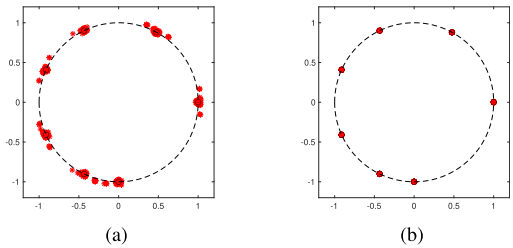

Fig. 8. Estimated roots of complex GD-TLS/F for 200 MC trials as the number of snapshots increases from (a) $\mathcal{K} = 10$ and (b) $\mathcal{K} = 100$, highlighting the convergence of the algorithm ($M = 12$, SNR $= 12$ dB).

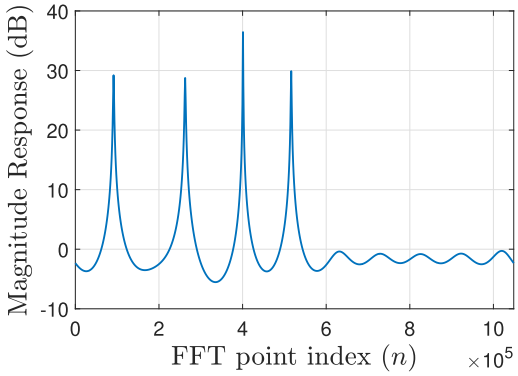

Fig. 9. Fourier domain spectrum of complex GD-TLS/F. The x-axis can be changed from the FFT point index to the θ domain by using the mapping in (27) to obtain the DOAs.

Finally, Fig. 9 shows the Fourier domain spectrum when the DOAs of the four sources are $10^\circ, 30^\circ, 50^\circ$ and 80°.

B. MSE Performance

In this subsection, we study the MSE performance of the proposed algorithms and compare them with complex LMS and complex GD-TLS. Fig. 10 shows the MSE convergence of all the algorithms for Case I. The figure shows that the proposed complex GD-TLS/F algorithm has the same convergence rate but with lower steady-state error compared to complex LMS, complex LMS/F and complex GD-TLS for SNR $= 6$ dB. This lower steady-state error will result in better DOA estimation performance. For SNR $= 14$ dB, the complex GD-TLS/F has the lowest steady-state error compared to all the other algorithms. From Fig. 10, we can also observe that complex LMS/F has lower steady-state error than complex LMS and complex GD-TLS/F has lower steady-state error than complex GD-TLS, which shows the advantage of the proposed family of complex least square/fourth algorithms. Furthermore, to validate the theoretical global optimal solution, we compared the theoretical MSE, computed using the proposed algorithm's globally optimal weight, with the simulated MSE. As shown in Fig. 11, the simulated MSE converges to the theoretical MSE as the number of snapshots increases, showing the optimality of the weight.

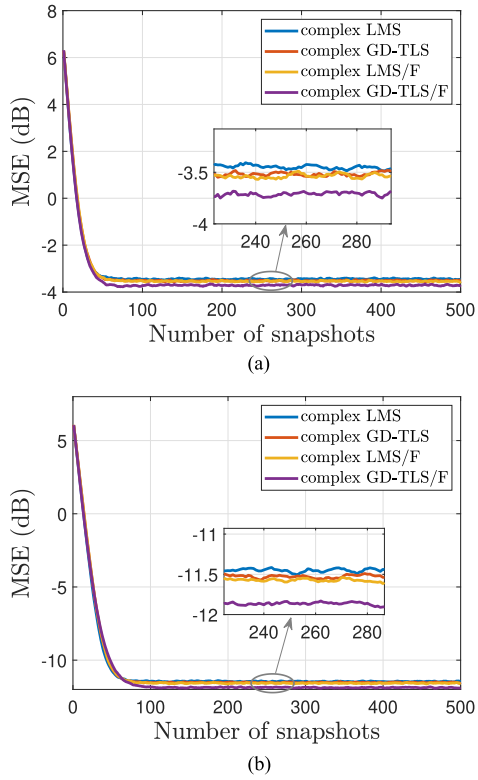

Fig. 10. MSE plot of complex LMS, complex GD-TLS, complex LMS/F and complex GD-TLS/F for SNR 6 dB and 14 dB ($M = 12$). (a) SNR $= 6$ dB. (b) SNR $= 14$ dB.

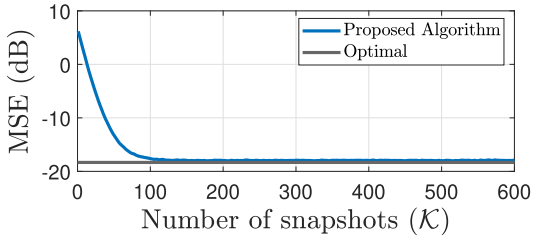

Fig. 11. Optimal and simulated MSE comparison for the proposed complex GD-TLS/F algorithm.

C. RMSE Performance

The performance of the algorithms using RMSE of estimated DOAs is studied in this subsection. The RMSE of the DOA estimation can be obtained as

$$\text{RMSE} = \sqrt{\frac{1}{LT}\sum_{l=1}^{L}\sum_{t=1}^{T}|(\theta_l - \theta_{l,t})|^2}, \qquad (64)$$

where $\theta_{l,t}$ is the estimated DOA of the l^{th} source in the t^{th} trial and θ_l is the actual DOA of the l^{th} source. T is the number of MC trials. The performances of the proposed algorithms are compared with complex LMS, complex GD-TLS, CBF, TLS-ESPRIT, MUSIC and root-MUSIC algorithms. The Cramer-Rao bound (CRB) is also plotted [46]. In Fig. 12(a), RMSE with increasing SNR is plotted for Case I. The proposed algorithm performs well as SNR increases from 6 dB to 22 dB. The RMSE performance comparison with increasing snapshots for Case I is

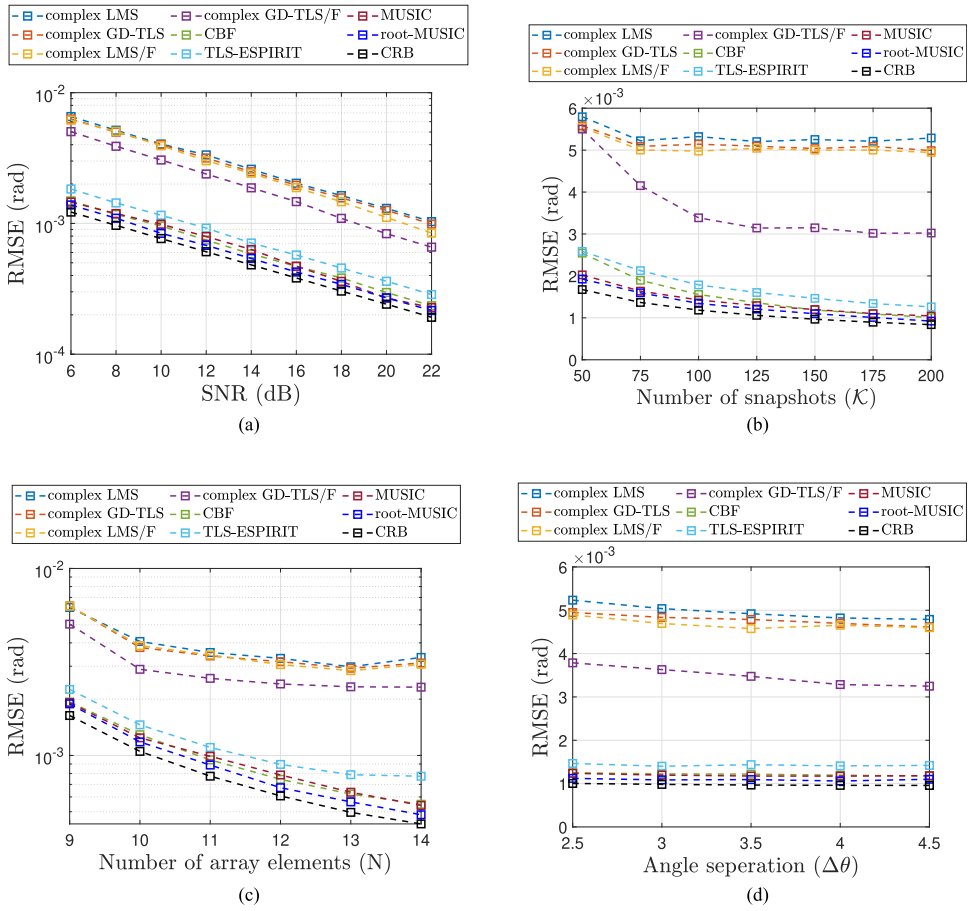

Fig. 12. RMSE of complex LMS, complex LMS/F, complex GD-TLS, complex GD-TLS/F, CBF, TLS-ESPRIT, MUSIC and root-MUSIC algorithm with respect to (a) SNR, (b) number of snapshots, (c) number of array elements and (d) angle separation, respectively. (a) $\mathcal{K} = 150$. (b) SNR $= 8$ dB. (c) SNR $= 12$ dB, $\mathcal{K} = 150$. (d) SNR $= 12$ dB, $\mathcal{K} = 150$.

shown in Fig. 12(b) for SNR $= 8$ dB. It can be seen that complex LMS/F and complex GD-TLS/F show good RMSE performance compared to complex LMS and complex GD-TLS for all the snapshots, with complex GD-TLS/F significantly outperforming the other adaptive algorithms. The RMSE plot with respect to the number of array elements is shown in Fig. 12(c). Once again, complex GD-TLS/F outperforms all the other adaptive algorithms for any number of array elements. The RMSE plot with respect to angle separation is shown in Fig. 12(d). The source directions for the simulation were considered to be $\theta = 0°, 30°, 34° + \Delta°, 50°$ where the angle separation $\Delta°$ varies from 2.5° to 4.5°. It can be observed that the proposed complex LMS/F algorithm performs better than complex LMS and complex GD-TLS. The proposed complex GD-TLS/F algorithm performs better than all the other adaptive algorithms for all the angle separations.

D. Probability of Detection Performance

Another metric to evaluate the performance of DOA estimation is the probability of Detection (PD). It is expressed as PD $= T_s/T$, where T_s is the number of successful estimations out of all the trials. In our simulation study, DOA estimation is considered to be successful if $|\theta_l - \theta_{l,t}| < 0.0012$ rd. In Fig. 13(a), the variation of PD with respect to SNR is shown for Case I. It can be observed that complex GD-TLS/F has better PD compared to other adaptive algorithms. To further evaluate the performance, the variation of PD with respect to the number of snapshots is plotted in Fig. 13(b). The figure shows that the PD of the proposed complex GD-TLS/F algorithm is better than all the other adaptive algorithms.

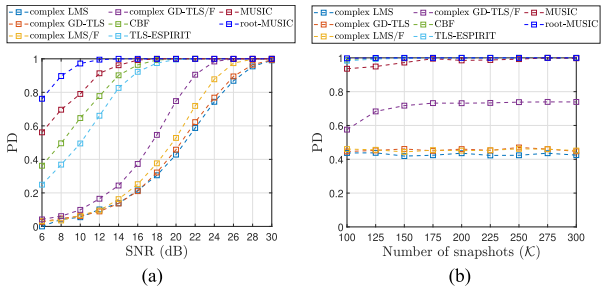

Fig. 13. PD of complex LMS, complex LMS/F, complex GD-TLS, complex GD-TLS/F, CBF, TLS-ESPRIT, MUSIC and root-MUSIC algorithm with respect to (a) SNR and (b) number of snapshots, respectively. (a) $\mathcal{K} = 200$. (b) SNR $= 24$ dB.

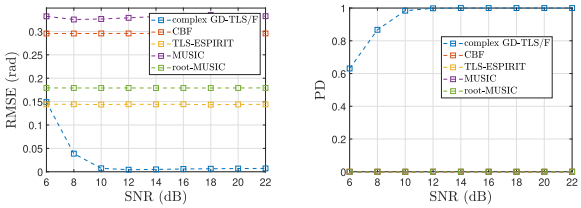

(a) (b)

Fig. 14. RMSE and PD of the algorithms with respect to SNR for change in source direction. (a) $\mathcal{K} = 700$. (b) $\mathcal{K} = 700$.

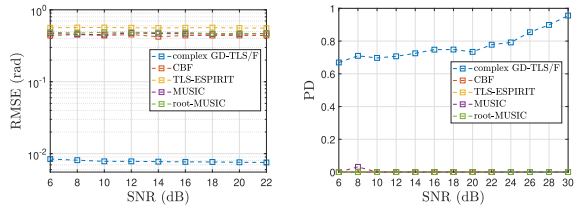

(a) (b)

Fig. 15. RMSE and PD of the algorithms with respect to SNR for correlated sources. (a) $\mathcal{K} = 200$. (b) $\mathcal{K} = 200$.

In RMSE and PD simulation results, although the subspace-based algorithms outperforms the adaptive algorithms, the computational complexity of subspace-based is of the order of $\mathcal{O}(M^3)$, while all the adaptive algorithms have a complexity of the order of $\mathcal{O}(M)$.

E. Performance Evaluation Under Changing Source Directions

Furthermore, simulations evaluating RMSE and PD were carried out, where the source directions shifted from $0°, 30°, 40°, 60°$ to $-30°, 5°, 35°, 45°$ at $\mathcal{K} = 350$. As illustrated in Fig. 14(a), subspace-based algorithms such as CBF, TLS-ESPRIT, MUSIC and root-MUSIC fail to track these dynamic changes, resulting in significant DOA estimation errors. By contrast, the proposed algorithm adapts successfully to the new source positions, showing lower RMSE under such conditions. Additionally, Fig. 14(b) highlights that subspace-based methods do not satisfy the PD success threshold of 0.015 rad due to their larger estimation errors, whereas the proposed algorithm exhibits a consistent improvement in PD performance when SNR is increased.

F. Performance Evaluation for Correlated Source Scenario

However, our proposed adaptive algorithm shows better performance than the subspace-based algorithms when the incoming signals are correlated. While subspace-based methods tend to fail under such conditions, the proposed adaptive framework is stable in updating its filter, allowing it to cope far more effectively, obtaining better DOA estimates. Fig. 15 shows the RMSE and PD performance of the proposed algorithm in comparison with CBF, TLS-ESPRIT, MUSIC and root-MUSIC algorithms. The figure shows that in the correlated-source scenario, the adaptive approach delivers lower RMSE and a higher detection probability than the subspace-based approaches.

VII. Conclusion

In this work, we proposed a family of Fourier domain complex least square/fourth adaptive algorithms for adaptive DOA estimation. The weight update rules for both the proposed algorithms, complex LMS/F and complex GD-TLS/F, are derived. An efficient method for obtaining the DOAs from the weights of the adaptive filter is also proposed based on the Fourier domain analysis of the weight vector. Further, we derive global optimal weight, mean stability, steady-state mean square performance and the condition for mean square convergence of the proposed algorithm. The comparative analysis in DOA estimation simulations shows that the proposed algorithms have lower steady-state error than the conventional complex LMS and complex GD-TLS algorithms. Additionally, the performances of the proposed algorithms show improved RMSE and detection performances when compared to existing algorithms.

References

[1] R. Schmidt, "Multiple emitter location and signal parameter estimation," *IEEE Trans. Antennas Propag.*, vol. TAP-34, no. 3, pp. 276–280, Mar. 1986.

[2] M. Rubsamen and A. B. Gershman, "Direction-of-arrival estimation for nonuniform sensor arrays: From manifold separation to fourier domain MUSIC methods," *IEEE Trans. Signal Process.*, vol. 57, no. 2, pp. 588–599, Feb. 2009.

[3] H. Abeida and J. -P. Delmas, "Resolving power of MUSIC-like algorithms for circular or rectilinear correlated sources in CES data models," *Signal Process.*, vol. 188, 2021, Art. no. 108234.

[4] R. Roy and T. Kailath, "ESPRIT-estimation of signal parameters via rotational invariance techniques," *IEEE Trans. Acoust., Speech, Signal Process.*, vol. 37, no. 7, pp. 984–995, Jul. 1989.

[5] D. D. Sartori, K. Adhikari, and R. J. Vaccaro, "Second-order optimal subspace estimation for ESPRIT-like DOA estimation," *Signal Process.*, vol. 217, 2024, Art. no. 109323.

[6] P. Stoica and K. C. Sharman, "Maximum likelihood methods for direction-of-arrival estimation," *IEEE Trans. Acoust., Speech, Signal Process.*, vol. 38, no. 7, pp. 1132–1143, Jul. 1990.

[7] H. Qiao and P. Pal, "On maximum-likelihood methods for localizing more sources than sensors," *IEEE Signal Process. Lett.*, vol. 24, no. 5, pp. 703–706, May 2017.

[8] P. Gerstoft, C. F. Mecklenbräuker, A. Xenaki, and S. Nannuru, "Multi-snapshot sparse Bayesian learning for DOA," *IEEE Signal Process. Lett.*, vol. 23, no. 10, pp. 1469–1473, Oct. 2016.

[9] J. Yang and Y. Yang, "Sparse Bayesian DOA estimation using hierarchical synthesis lasso priors for off-grid signals," *IEEE Trans. Signal Process.*, vol. 68, pp. 872–884, 2020.

[10] R. R. Pote and B. D. Rao, "Maximum likelihood-based gridless DOA estimation using structured covariance matrix recovery and SBL with grid refinement," *IEEE Trans. Signal Process.*, vol. 71, pp. 802–815, 2023.

[11] A. Xenaki, J. B. Boldt, and M. G. Christensen, "Sound source localization and speech enhancement with sparse Bayesian learning beamforming," *J. Acoustical Soc. Amer.*, vol. 143, no. 6, pp. 3912–3921, 2018.

[12] H. Zhang, D. Xu, and N. Wang, "Explicit performance limit for joint range and direction of arrival estimation in phased-array radar sensors," *IEEE Trans. Veh. Technol.*, vol. 72, no. 11, pp. 14289–14304, Nov. 2023.

[13] H. Fu, F. Dai, and L. Hong, "Off-grid error calibration for DOA estimation based on sparse Bayesian learning with weighted sinc interpolation," *IEEE Trans. Veh. Technol.*, vol. 72, no. 12, pp. 16293–16307, Dec. 2023.

[14] F. Yang, S. Yang, L. Sun, Y. Chen, S. Qu, and J. Hu, "DOA estimation via sparse signal recovery in 4-D linear antenna arrays with optimized time sequences," *IEEE Trans. Veh. Technol.*, vol. 69, no. 1, pp. 771–783, Jan. 2020.

[15] X. Wang, D. Meng, M. Huang, and L. Wan, "Reweighted regularized sparse recovery for DOA estimation with unknown mutual coupling," *IEEE Commun. Lett.*, vol. 23, no. 2, pp. 290–293, Feb. 2019.

[16] E. T. Northardt, I. Bilik, and Y. I. Abramovich, "Spatial compressive sensing for direction-of-arrival estimation with bias mitigation via expected likelihood," *IEEE Trans. Signal Process.*, vol. 61, no. 5, pp. 1183–1195, Mar. 2013.

[17] Q. Shen, W. Liu, W. Cui, and S. Wu, "Underdetermined DOA estimation under the compressive sensing framework: A review," *IEEE Access*, vol. 4, pp. 8865–8878, 2016.
[18] S. Uehashi, Y. Ogawa, T. Nishimura, and T. Ohgane, "Prediction of time-varying multi-user MIMO channels based on DOA estimation using compressed sensing," *IEEE Trans. Veh. Technol.*, vol. 68, no. 1, pp. 565–577, Jan. 2019.
[19] H. Zamani, H. Zayyani, and F. Marvasti, "An iterative dictionary learning-based algorithm for DOA estimation," *IEEE Commun. Lett.*, vol. 20, no. 9, pp. 1784–1787, Sep. 2016.
[20] P. Chen, Z. Chen, Z. Cao, and X. Wang, "A new atomic norm for DOA estimation with gain-phase errors," *IEEE Trans. Signal Process.*, vol. 68, pp. 4293–4306, 2020.
[21] Y. Wu, M. B. Wakin, and P. Gerstoft, "Gridless DOA estimation with multiple frequencies," *IEEE Trans. Signal Process.*, vol. 71, pp. 417–432, 2023.
[22] X. Zhang, Z. Zheng, W. -Q. Wang, and H. C. So, "DOA estimation of coherent sources using coprime array via atomic norm minimization," *IEEE Signal Process. Lett.*, vol. 29, pp. 1312–1316, 2022.
[23] Z. Yang and L. Xie, "Enhancing sparsity and resolution via reweighted atomic norm minimization," *IEEE Trans. Signal Process.*, vol. 64, no. 4, pp. 995–1006, Feb. 2016.
[24] M. Wagner, Y. Park, and P. Gerstoft, "Gridless DOA estimation and root-MUSIC for non-uniform linear arrays," *IEEE Trans. Signal Process.*, vol. 69, pp. 2144–2157, 2021.
[25] H. Zeng, Z. Ahmad, J. Zhou, Q. Wang, and Y. Wang, "DOA estimation algorithm based on adaptive filtering in spatial domain," *China Commun.*, vol. 13, no. 12, pp. 49–58, Dec. 2016.
[26] B. Jalal, X. Yang, X. Wu, T. Long, and T. K. Sarkar, "Efficient direction-of-arrival estimation method based on variable-step-size LMS algorithm," *IEEE Antennas Wireless Propag. Lett.*, vol. 18, no. 8, pp. 1576–1580, Aug. 2019.
[27] H. Zhao, W. Luo, Y. Liu, and C. Wang, "A variable step size gradient-descent TLS algorithm for efficient DOA estimation," *IEEE Trans. Circuits Syst. II: Exp. Briefs*, vol. 69, no. 12, pp. 5144–5148, Dec. 2022.
[28] S. Joel, K. Kumar, and N. V. George, "Robust DOA estimation based on an exponential hyperbolic cosine adaptive algorithm," *IEEE Sens. Lett.*, vol. 7, no. 5, May 2023, Art. no. 7001904.
[29] C. Liu and H. Zhao, "Efficient DOA estimation method using bias-compensated adaptive filtering," *IEEE Trans. Veh. Technol.*, vol. 69, no. 11, pp. 13087–13097, Nov. 2020.
[30] B. Jalal, O. Elnahas, X. Xu, Z. Quan, and P. Zhang, "Robust DOA estimation using VSS-LMS with low rank matrix approximation," *IEEE Trans. Aerosp. Electron. Syst.*, vol. 59, no. 3, pp. 2967–2978, Jun. 2023.
[31] B. Jalal, X. Yang, D. Igambi, T. Ul Hassan, and Z. Ahmad, "Low complex direction of arrival estimation method based on adaptive filtering algorithm," *J. Eng.*, vol. 2019, no. 19, pp. 6214–6217, 2019.
[32] S. Joel, S. K. Yadav, and N. V. George, "Adaptive low-rank DOA estimation using complex Kronecker product decomposition," *IEEE Trans. Veh. Technol.*, vol. 73, no. 7, pp. 10726–10731, Jul. 2024.
[33] B. Jalal, O. Elnahas, and Z. Quan, "Efficient DOA estimation under partially impaired antenna array elements," *IEEE Trans. Veh. Technol.*, vol. 71, no. 7, pp. 7991–7996, Jul. 2022.
[34] S. Joel, S. K. Yadav, and N. V. George, "Coarray LMS: Adaptive underdetermined DOA estimation with increased degrees of freedom," *IEEE Signal Process. Lett.*, vol. 31, pp. 591–595, 2024.
[35] S. Zhang, H. Zhao, and H. C. So, "Delayed combination of adaptive filters in colored noise," *IEEE Trans. Signal Process.*, vol. 70, pp. 1918–1931, 2022.
[36] S. Joel, M. L. N. S. Karthik, S. K. Yadav, and N. V. George, "Adaptive direction of arrival estimation using sparsity constrained complex NLMS algorithm with variable penalty factor," *IEEE Trans. Veh. Technol.*, vol. 74, no. 8, pp. 12603–12615, Aug. 2025.
[37] H. Zhao, Y. Peng, and W. Xu, "Complex total maximum Versoria criterion algorithm for DOA estimation," *IEEE Trans. Circuits Syst. II: Exp. Briefs*, vol. 71, no. 4, pp. 2489–2493, Apr. 2024.
[38] O. M. Abdelrhman, S. Li, Y. Dou, and L. Bin, "Robust total maximum versoria algorithm for efficient DOA estimation in noisy inputs," *IEEE Trans. Veh. Technol.*, vol. 73, no. 10, pp. 15087–15097, Oct. 2024.
[39] E. Walach and B. Widrow, "The least mean fourth (LMF) adaptive algorithm and its family," *IEEE Trans. Inf. Theory*, vol. TIT-30, no. 2, pp. 275–283, Mar. 1984.
[40] J. Harris et al., "Combined LMS/F algorithm," *Electron. Lett.*, vol. 33, no. 6, pp. 467–468, 1997.
[41] M. Karthik, S. Pradhan, and N. V. George, "Performance evaluation of an active headrest system using a filtered-x least mean square/fourth algorithm with virtual sensing," *J. Acoustical Soc. Amer.*, vol. 154, no. 5, pp. 2878–2891, 2023.
[42] Y. Li, Y. Wang, and T. Jiang, "Norm-adaption penalized least mean square/fourth algorithm for sparse channel estimation," *Signal Process.*, vol. 128, pp. 243–251, 2016.
[43] Lim and J. G. Harris, "Combined LMS/F algorithm," *Electron. Lett.*, vol. 33, no. 6, pp. 467–468, 1997.
[44] A. H. Sayed, *Adaptive Filters.* Hoboken, NJ, USA: Wiley, 2011.
[45] P. S. Diniz et al., *Adaptive Filtering*, vol. 4. Berlin, Germany: Springer, 1997.
[46] A. H. Sayed, *Fundamentals of Adaptive Filtering.* Hoboken, NJ, USA: Wiley, 2003.
[47] C. Liu and M. Jiang, "Robust adaptive filter with lncosh cost," *Signal Process.*, vol. 168, 2020, Art. no. 107348.

Joel S. (Graduate Student Member, IEEE) received the Bachelor of Technology degree in electrical and electronics engineering from the University of Kerala, Thiruvananthapuram, India, in 2017, and the Master of Technology degree in electrical engineering from the National Institute of Technology, Hamirpur, India, in 2020. He is currently working toward the Ph.D. degree with the Department of Electrical Engineering, Indian Institute of Technology Gandhinagar, Gandhinagar, India. His research focuses on adaptive, and array signal processing.

Shekhar Kumar Yadav (Member, IEEE) received the Bachelor of Engineering degree in electrical and electronics engineering from the Birla Institute of Technology and Science Pilani, Pilani, India, in 2015, and the Ph.D. degree in electrical engineering from the Indian Institute of Technology Gandhinagar, Gandhinagar, India, in 2023. He was a Research Associate with the Indian Institute of Technology Gandhinagar from 2023 to 2024. He is currently a Postdoctoral Research Fellow with the Audio Information Processing Lab, Technical University of Munich, Munich, Germany. His research interests include multichannel signal processing, DOA estimation, acoustic beamforming, and audio processing.

Munukutla L. N. Srinivas Karthik received the Bachelor of Technology degree in electronics and communication engineering from Jawaharlal Nehru Technological University, Hyderabad, India, in 2016, and the Master of Technology degree in communication and signal processing engineering from the International Institute of Information Technology, Bhubaneswar, India, in 2018. He is currently working toward the Ph.D. degree with the Department of Electrical Engineering, Indian Institute of Technology Gandhinagar, Gandhinagar, India. His research interests include signal processing theory, audio and speech processing, active noise control.

Nithin V. George (Member, IEEE) received the Bachelor of Technology degree in electronics and communication engineering from the University of Kerala, Thiruvananthapuram, India, in 2007, the Master of Technology degree in telematics and signal processing from the National Institute of Technology Rourkela, Rourkela, India, in 2009, and the Ph.D. degree in electrical sciences from the Indian Institute of Technology Bhubaneswar, Bhubaneswar, India, in 2012. He is currently a TEOCO Chair Professor with the Department of Electrical Engineering, Indian Institute of Technology Gandhinagar, Gandhinagar, India. His research interests include active noise control, adaptive signal processing, array signal processing, assistive listening devices, and psychoacoustics. He was the recipient of the Department of Foreign Affairs and International Trade, Government of Canada, GSEP Fellowship, in 2008, the INSPIRE Faculty Award in 2013, and the Indo-Australia Early and Mid-Career Researcher's Fellowship in 2017. He was an Associate Editor for the *Swarm and Evolutionary Computation* journal from 2016 to 2020.